ELSEVIER

Physica B 249–251 (1998) 628–635

PHYSICA B

Magnetotransport in the two-dimensional electron fluid and solid on liquid helium

M.J. Lea[a,*], M.I. Dykman[b]

[a] *Department of Physics, Royal Holloway, University of London, TW20 0EX, UK*
[b] *Department of Physics and Astronomy, Michigan State University, MI 48824, USA*

Abstract

We present measurements and theory of the magnetoconductivity $\sigma(B)$ of the 2D electron fluid and Wigner crystal above the surface of liquid helium. Many-electron effects give rise to (i) Drude behaviour $\sigma(B) = \sigma(0)/(1 + \mu^2 B^2)$, even in classically strong fields, $\mu B \gg 1$ (μ is the zero-field mobility), (ii) saturation and density dependence of $\sigma(B)/\sigma(0)$ above an onset field B_0, which depends on the fluctuational internal electric field $\boldsymbol{E}_f$, (iii) an increase in $\sigma(B)$ in quantising fields. Far in the quantum limit, single-particle scattering dominates. For typical electron densities, $\sigma(B) \propto T^{-1/2}$ for $B > 2$ T and $T < 0.6$ K, which is as expected for ripplon scattering, and does not change at the melting transition at T_m. In low fields in the Wigner solid on ^{4}He, $\sigma(B)$ is non-linear due to the Bragg–Çerenkov radiation of coherent ripplons, which limits the Hall velocity to v_1, the phase velocity of the ripplons at the first reciprocal lattice vector. Above a threshold drive voltage, $\sigma(B)$ decreases sharply. Above T_m, fluctuations in $\sigma(B)$ are observed below a temperature $T_f = (2.8 \pm 0.3)T_m$ indicating that some aspects of the 2D electron solid might persist to well above the melting temperature.

Keywords: Liquid helium; Magnetoconductance; Magnetotransport

1. Introduction

Electrons in surface states above liquid helium form an almost ideal two-dimensional conductor [1]. For a typical interelectron distance of 1 μm the electrons are highly correlated, in a normal electron fluid or a Wigner crystal, with a melting transition at $\Gamma = e^2(\pi n)^{1/2}/4\pi\varepsilon_0 kT = 127 \pm 3$ [2] (n is the electron density and the plasma parameter Γ is the ratio of potential and kinetic energies). The phase diagram is shown in Fig. 1.

The electron dynamics in a non-degenerate electron fluid are qualitatively different from a non-interacting ideal gas. The electron motion is a combination of vibrations in a potential well (which is related to short-range order) and self-diffusion. In the Wigner crystal, the diffusion ceases. The characteristic angular frequency of vibration is $\omega_p = (e^2 n^{3/2}/2\varepsilon_0 m)^{1/2} = 39.9\, n^{3/4}$ rad/s. The temperature $T_p = \hbar\omega_p/k$ is shown in Fig. 1. For $T > T_p$ the electron vibrations are classical, while for $T < T_p$, they are quantised, in both the fluid and

* Corresponding author. Fax: + 44 1784 472794; e-mail: m.lea@rhbnc.ac.uk.

0921-4526/98/$19.00
PII: S0921-4526(98)00274-9

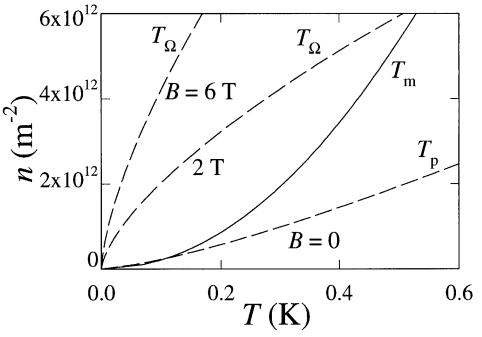

Fig. 1. The melting temperature T_m for 2D electrons on helium. The classical ($B = 0$) and semi-classical ($B = 2$ and 6 T) regions lie to the right of the dashed lines.

the solid. This crossover occurs close to T_m for $n < 10^{12}\ m^{-2}$ (Fig. 1).

In a magnetic field B, the characteristic vibrational frequency becomes $\Omega = \omega_p^2/\omega_c$ for $\omega_p \ll \omega_c = eB/m$, the cyclotron frequency. The characteristic temperature $T_\Omega = \hbar\Omega/k$ is shown in Fig. 1 for $B = 2$ and 6 Tesla. For $T > T_\Omega$, the electronic motion becomes semi-classical, with the centres of the cyclotron orbits (radius the magnetic length $l_B = (\hbar/eB)^{1/2}$) moving as classical objects with vibrational frequency Ω. This magnetically induced semiclassical region may extend to very low temperatures, well into the solid.

A key role in the theory of the magnetoconductivity in the classical and semi-classical region is played by the internal field $\boldsymbol{E}_f$ which is seen by each electron and arises due to electron density fluctuations [3,4]. The rms field $\langle E_f^2\rangle^{1/2}$ has been found from Monte Carlo simulations [5] and is given by $\langle E_f^2\rangle = F(\Gamma)E_0^2$, where $E_0^2 = kTn^{3/2}/4\pi\varepsilon_0$. The numerical parameter $F(\Gamma) \approx 9$ is a weak function of Γ, only changing slightly through the melting transition.

The electrons are scattered by helium vapour atoms (above 1 K) and by ripplons on the helium surface. Since the vapour density varies exponentially with T, the mobility μ changes by many decades with temperature. In the classical and semiclassical domains in Fig. 1, the scattering is short range. The magnetoconductivity $\sigma(B)$ is measured using Corbino disk electrodes under an electron sheet [1,6] or extracted from the damping of edge magnetoplasmons [7,8].

Several regions of magnetoconductivity can be distinguished. In weak and moderately strong (including classically strong) magnetic fields in the fluid, $\sigma(B)$ is described by the Drude formula, due to many-electron effects [9,10]. In stronger classical, and also in quantising fields, the ratio $\sigma(B)/\sigma(0)$ becomes explicitly density dependent. At still higher fields there occurs a crossover to independent electron scattering [3,4,9,10].

For a 2D solid on liquid ^{4}He, even for weak driving fields and small B, the transport is non-linear due to coherent Bragg–Çerenkov radiation of ripplons [11,12]. Some features of this may extend above T_m and give rise to new effects in an inhomogeneous 2D electron phase [13]. But the 2D solid on ^{3}He [14] does not display the same non-linearity and follows the Drude model in both fluid and solid. Shirahama et al. [15] have also recently observed the scattering of ^{3}He quasiparticles from the 2D Wigner solid on superfluid ^{3}He in zero field.

2. The Drude region (weak and moderately strong fields)

Iye [16] first showed experimentally that $\sigma(B)$ is described by the Drude model

$$\sigma(B) = \frac{\sigma(0)}{1 + \mu^2 B^2} \approx \frac{ne}{\mu B^2} \tag{1}$$

up to classically strong fields as confirmed later by several groups [6,14,17] see Fig. 2 [18]. It is surprising that this holds for $\mu B \gg 1$, when Landau level quantisation should change the density of states and quasi-elastic scattering by ripplons or vapour atoms becomes forbidden, in lowest order perturbation theory. Many-electron effects restore the Drude model [4,9,10] as the kinetic energy of an electron wave packet is smeared in the fluctuational field by $eE_f\hat{\lambda}_T$, ($\hat{\lambda}_T$ is the thermal de Broglie wavelength). For $e\langle E_f^2\rangle^{1/2}\hat{\lambda}_T \gg \hbar\omega_c$, this washes out the Landau quantisation for a quasi-elastic scattering of an electron in the field of other electrons. Experimental Drude mobilities agree well with zero field measurements, though there are often slightly lower than the theoretical values [6,14].

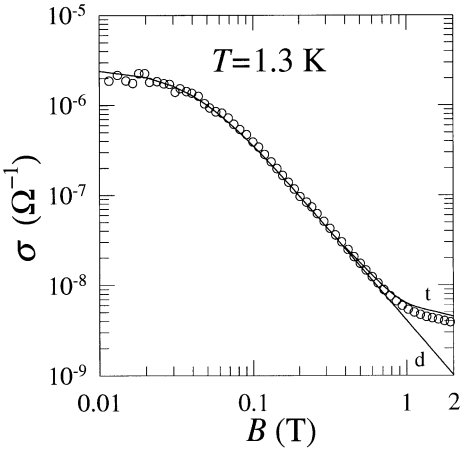

Fig. 2. The Drude model (**d**) for $n = 0.64 \times 10^{12}\ \mathrm{m}^{-2}$ at 1.3 K, $\mu = 24\ \mathrm{m}^2/\mathrm{V\,s}$.

3. Strong fields

3.1. Saturation of the magnetoconductivity

For B beyond the Drude region, $\sigma(B)$ first saturates and then increases again as in Fig. 3 at 0.7 K in the ripplon scattering regime. Deviations from Eq. (1) become substantial where an electron repeatedly collides with the same short-range scatterer because, for a given B, the fluctuational field

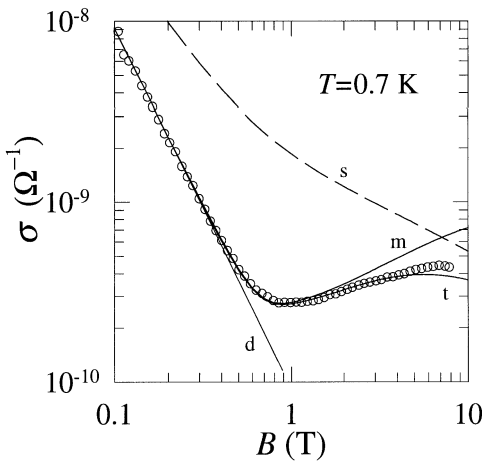

Fig. 3. The magnetoconductivity $\sigma(B)$ for $n = 0.55 \times 10^{12}\ \mathrm{m}^{-2}$ at 0.7 K in the 2D electron fluid. Theory lines are shown: **d**: Drude model, **s**: SCBA, **m**: many-electron and **t**: total.

$\boldsymbol{E}_\mathrm{f}$ is not strong enough to drive it away from the scatterer, over a cyclotron period, by a distance exceeding the size of the electron wavepacket $\hat{\lambda}_\mathrm{T}$. This defines an onset field for magnetoresistance $B_0 = [2\pi m^3 kT/\hbar^2 e^2 \langle E^{-1}\rangle^2]^{1/4}$ which lies in the range 0.2–1 tesla. At saturation, for $B \gg B_0$, $\sigma(B) = ne/\pi\mu B_0^2$ for a δ-correlated random potential. Measurements of σ for $B \geqslant B_0$ give the fluctuational field E_f [19].

The many-electron quantum transport equation [4] gives for $\omega_c\tau \gg 1$

$$\sigma = \frac{ne^2}{4m^2\omega_c^2 kT}\sum_{\boldsymbol{q}} q^2 \overline{|V_{\boldsymbol{q}}|^2}\,\xi(\boldsymbol{q}) \tag{2}$$

where $\overline{|V_{\boldsymbol{q}}|^2}$ is the mean square Fourier component of the scattering field, and $\xi(\boldsymbol{q})$ is the electron density correlator. For $B > B_0$ and arbitrary $B/B_T = \hbar\omega_c/kT$

$$\xi(\boldsymbol{q}) = \frac{2\tau_\mathrm{e}}{l_B q}\exp[-q^2 l_B^2(2\bar{n}+1)/2] \times \sum_{m=0}^{\infty}\left(\frac{q^2 l_B^2}{2}\right)^{2m}\frac{[\bar{n}(\bar{n}+1)]^m}{(m!)^2},$$

$$\tau_\mathrm{e} = B l_B \langle E_\mathrm{f}^{-1}\rangle \tag{3}$$

where $\bar{n} = [\exp(B/B_T) - 1]^{-1}$ is the Planck number. For $\bar{n} \ll 1$ (the ultraquantum limit) only one term (with $m = 0$) should be kept in the sum. The characteristic size of the electron wave packet is then l_B and τ_e gives the time of flight of an electron past a short-range scatterer in the crossed $\boldsymbol{B}$ and $\boldsymbol{E}_\mathrm{f}$ fields.

In the case of ripplon scattering, Eq. (2) applies provided the electron drift velocity E_f/B exceeds the phase velocity ω_q/q of ripplons with wave vectors $q \sim 1/l_B$. Otherwise the Çerenkov scattering rate is suppressed. For an arbitrary ratio of the velocities and for a Gaussian distribution of the field $\boldsymbol{E}_\mathrm{f}$ [5] the factor $\xi(\boldsymbol{q})$ is renormalised as (for $\bar{n} \ll 1$, $kT \gg \hbar\omega_q$).

$$\xi(\boldsymbol{q}) \to \xi(\boldsymbol{q})\exp[-\pi^{-1}(\omega_q\tau_\mathrm{e}/l_B q)^2]. \tag{4}$$

The related decrease of σ at low densities n was observed in Ref. [7].

For non-quantising fields, $B < B_T$, but for arbitrary B/B_0

$$\xi(\boldsymbol{q}) = \left(\frac{2\pi m}{kTq^2}\right)^{1/2} \exp\left[-\frac{\hbar^2 q^2}{8mkT}\right] \times \sum_{s=-\infty}^{\infty} \exp\left(-\frac{\pi^2 s^2 \hbar^2 q^2 B_0^4}{2mkTB^4}\right) \quad (5)$$

again assuming that the distribution of $\boldsymbol{E}_f$ is Gaussian. Eq. (5) goes over into the high-field limit of the Drude formula, Eq. (1) for $B \ll B_0$.

For ripplon scattering, $\overline{|V_q|^2} = S^{-1}(kTe^2/\alpha q^2)[E_z + E_{pol}(q)]^2$, where α is the surface tension, E_z is the vertical pressing field, $E_{pol}(q) = (\hbar^2\gamma^{(0)}/2me)q^2\phi(q/2\gamma)$ is the effective interaction field due to polarisation charges, γ and $\gamma^{(0)}$ (1.3×10^{-8} m) are the inverse localisation lengths of the electron wave function perpendicular to the surface with and without the pressing field, and $\phi(x) = (x^2-1)^{-1} - (x^2-1)^{-3/2}\tan^{-1}[(x^2-1)^{1/2}]$ for $x > 1$ (the value of $\phi(x)$ for $x < 1$ can be obtained by analytic continuation).

Theoretical values for the many-electron $\sigma(B)$ in the classical and quantum regions are shown in Fig. 3 and give a good account of the data for fields lower than 5 T. These many-electron effects have also been observed in the damping of edge magnetoplasmons in the gas–atom scattering region [8].

3.2. Independent electrons – the method of moments

For higher fields and temperatures, the scattering rate is no longer small compared to the reciprocal collision duration. Many-electron effects are then less significant [3], and the conductivity can be treated in the independent electron approximation. Several approximate methods have been used to describe this strong-coupling regime. The self-consistent Born approximation (SCBA) has been given for gas–atom scattering in Ref. [20] and a modified version for ripplon scattering by Saitoh [21] for $B > B_T$. For gas–atom scattering, the SCBA agrees well with data by Tress [17] for $B \leqslant 20$ tesla. The ripplon SCBA plotted in Fig. 3 (the original explicit expressions [21], used in our previous papers [6], have been extended to arbitrary γl_B) approaches the data at the highest fields.

An alternative, asymptotically exact approach to the analysis of magnetoconductivity is based on the method of moments, where σ is obtained from the integrals of ω^n weighted with the frequency-dependent conductivity σ_ω. The function σ_ω has a peak of width $\sim \tau^{-1}$ at the frequency $\omega = 0$, and it is the shape of this peak that can be analysed using the method of moments. In the short-range scattering region, the method of moments confirms the SCBA to a very good accuracy, $\leqslant 5\%$ [22]. There is also good agreement between the method of moments and the results [21] for the contributions from the short-range term $\propto E_z E_{pol}$ in the electron–ripplon coupling. However, for the term $\propto E_z^2$ the difference is quite substantial, up to 30%.

3.3. The transition to the solid phase

An interesting feature of the electron transport in the classical and semiclassical domains in Fig. 1 is that the many-electron scattering rate is determined essentially by the short-range order in the electron system. Therefore the conductivity and cyclotron resonance should not change significantly when the system melts. In particular, for quantising fields ($B > B_T$) the calculations [23,24] in terms of many-phonon decay of the phonons of a Wigner crystal give the same expressions for the magnetotransport coefficients as Eqs. (2) and (3), while the parameter of the many-electron theory $\langle E_f^2\rangle^{1/2}$ changes by less than 1% at the melting transition.

The temperature dependence of the magnetoconductivity $\sigma(B)$ in a fixed quantising magnetic field ($B = 2$ T) is shown in Fig. 4 for $n = 1.85 \times 10^{12}$ m^{-2} [25]. Below 0.6 K, ripplons are the dominant scattering mechanism, Eq. (4). It follows from Eqs. (2) and (3), with account taken of $\tau_e \propto \langle E_f^{-1}\rangle \propto T^{-1/2}$ that in this range $\sigma \propto T^{-1/2}$. The same temperature dependence is obtained for the SCBA but with a different prefactor. The lines in Fig. 4 show the theoretical $\sigma(B)$. Remarkably there is only a small change in $\sigma(B)$ at the melting temperature T_m (0.30 K), and the temperature dependence is the same in the liquid and solid phases.

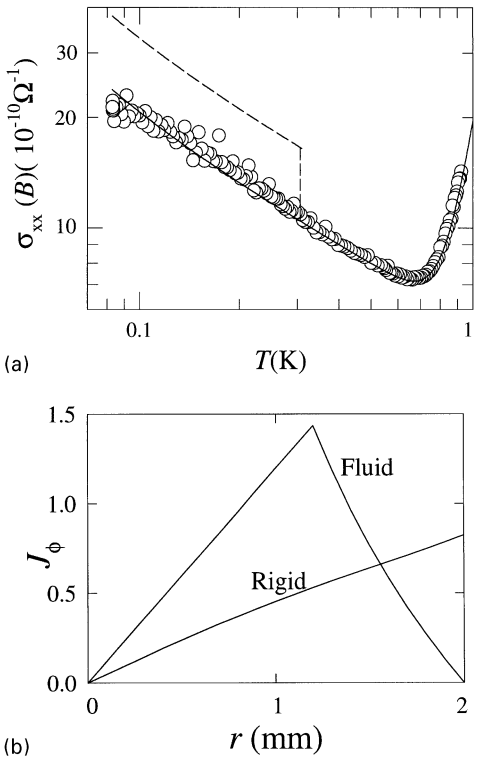

Fig. 4. (a) The temperature dependence of $\sigma(B)$ for $n = 1.85 \times 10^{12}\,\mathrm{m}^{-2}$ at 2 Tesla. The solid line shows the many-electron theory for gas–atom and ripplon scattering. The melting temperature is at $T_\mathrm{m} = 0.30$ K. The dashed line shows the effective conductivity for rigid rotation. (b) The azimuthal $J_\phi(r)$ current density in the Corbino disk for (i) fluid rotation ($= \omega_c \tau J_r(r)$) and (ii) rigid rotation (arbitrary units).

3.4. The shear modulus

The continuity of the measured $\sigma(B)$ through melting presents a paradox. The conductivity is obtained from the phase shift using Corbino electrodes (Fig. 6) in which a central electrode is driven with a AC($1 < f < 100$ kHz) voltage V_0 and the AC current to outer receiving electrodes is measured. For low phase shifts, $\theta = A/\sigma$, where the constant A assumes a local, homogeneous conductivity, as for a fluid [6]. The capacitatively coupled radial current density $J_r(r)$ produces a Lorentz force $J_r(r)B$ which drives an azimuthal current density $J_\phi(r) = \omega_c \tau J_r(r)$, Fig. 4b. But the crystal should be expected to rotate rigidly, with $J_\phi(r) \propto r$, giving a non-local response.

The analysis of the response of the crystal can be done in terms of the long-wavelength transmission line modes [26]. Their dispersion law has been obtained for wavelengths exceeding the depth d of the electrons above the screening electrodes, for a free boundary of the electron layer (zero shear stress at the perimeter of the Corbino disc). The parameter β that characterizes the dispersion relations is given by the squared product of the ratio of the transverse and longitudinal sound velocities c_t/c_l (which is small) times the ratio of the conductivities σ_{xy}/σ_{xx} (which is large), so that in the experimental conditions $\beta \approx 1$.

For the system investigated experimentally (see Fig. 4) the effect of rigid rotation produced by the shear modulus, for small phase shifts, is to reduce the losses, as compared to a fluid, by a geometrical factor of 0.60 for the same scattering rate [26]. The effective measured conductivity should increase by $\approx 40\%$ at T_m, as calculated in Fig. 4 (dashed line), but this is not seen experimentally. Neither do we see the associated change in current amplitude at the melting transition. The continuity of the temperature dependence confirms that the electrons are below T_m. We conclude that the solid is not rotating rigidly but may be polycrystalline, that slip occurs and that our measurements give the true local conductivity $\sigma(B)$.

4. Bragg–Çerenkov scattering

4.1. Hall-velocity limited magnetoconductivity

At low fields B in the solid, where quantisation of short-wavelength electron vibrations is substantial, the situation changes dramatically. Shirahama and Kono [27] showed that the magnetoconductivity is highly non-linear for electrons on ^{4}He (unlike the semiclassical region considered above and electrons on ^{3}He [14]). Experiments by Kristensen et al. [11] found that, for a broad range of driving voltages V_0, the measured effective Corbino magnetoconductivity in the solid, σ_s, was closely given by the semi-empirical relation

$$\sigma_s = (KfV_0/v_1Bd) \tag{6}$$

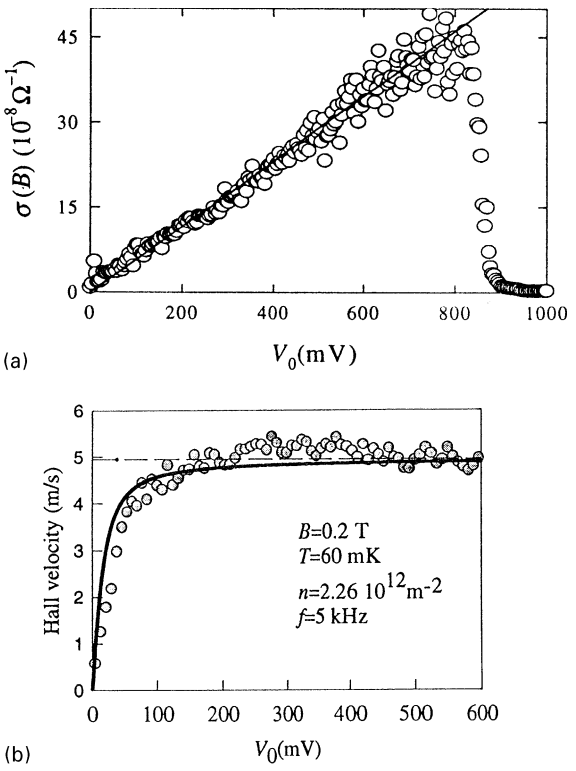

Fig. 5. (a) The magnetoconductivity $\sigma(B)$ for $n = 2.26 \times 10^{12}\,\mathrm{m}^{-2}$ in the solid at 60 mK, versus the drive voltage V_0. The line shows Eq. (6). (b) The experimental Hall velocity versus V_0. The solid line shows the Bragg–Çerenkov theory [12].

for the frequency, drive amplitude and magnetic field dependence of σ_s, where $v_1 = (\alpha G_1/\rho)^{1/2}$ is the ripplon phase velocity at the first reciprocal lattice vector $G_1 = (8\pi^2 n/\sqrt{3})^{1/2}$ of the Wigner crystal, K is a geometrical constant and ρ is the density of the helium. Data for $n = 2.26 \times 10^{-12}\,\mathrm{m}^{-2}$ are shown in Fig. 5a. The conductivity increases almost linearly up to a threshold voltage.

The effect was explained [12] as the Bragg–Çerenkov scattering, coherent many-electron emission (absorption) of ripplons by the moving lattice, which resonantly increases the drag force as the azimuthal Hall velocity (in the Corbino disk) approaches v_1. This increase is substantially related to the absence of long-range translational order in a 2D solid: for an infinite system the drag force increases as $|\boldsymbol{G}_1 \cdot \boldsymbol{v} - G_1 v_1|^{-1+\alpha(G_1)}$ for small $|\boldsymbol{G}_1 \cdot \boldsymbol{v} - G_1 v_1|$ where $\boldsymbol{v}$ is the crystal velocity (essentially, the Hall velocity), and $\alpha(G) = kTG^2/4\pi m c_t^2$ is the characteristic parameter for the smearing of Bragg peaks in the density correlator of 2D systems. This locks the Hall velocity to v_1 in a broad range of driving voltages V_0 and leads to Eq. (6). In the limit of small V_0 the conductivity is independent of V_0 and is determined by many-phonon scattering by ripplons.

4.2. The conductivity threshold

Wilen and Giannetta [28] discovered hysteresis in the solid magnetoconductivity, now studied in detail by Shirahama and Kono [27, 29, 30] who found a threshold voltage $V_c \propto n^{1.5} E_z / f B^{0.8}$ and mapped out a dynamic phase diagram with two solid phases: (i) the usual 2D solid with coupled plasmon-ripplon (CPR) modes and (ii) an uncoupled 2D solid moving freely over the helium surface. They proposed a simple model for the maximum force on an electron displaced in the small dimple under each localised electron in the 2D crystal. This accounts for some features of the breakdown but underestimates V_c. We have measured the threshold voltage at higher fields and find (i) for quantising fields, $B > B_T$, above 0.1 T, V_c is almost independent of B, in contrast to lower fields [27], (ii) the non-linearities and the threshold become weaker as B increases and above 2 T the response is linear and no clear threshold is observed, (iii) V_c is a strong function of the pressing field E_z. One of the reasons for the breakdown may be the finite size of crystallites: the maximum friction force due to the Bragg–Çerenkov scattering would be determined by this size, and breakdown could occur when the drag force exceeds this maximum.

4.3. Amomalous behaviour above the melting temperature

Another striking effect in the low field region is that some aspects of the unusual conductivity of the 2D electron solid extend to well above T_m. Fig. 6 shows the temperature dependence of $\sigma(B)$ at 0.2 T. Above 0.7 K the conductivity is given by the Drude

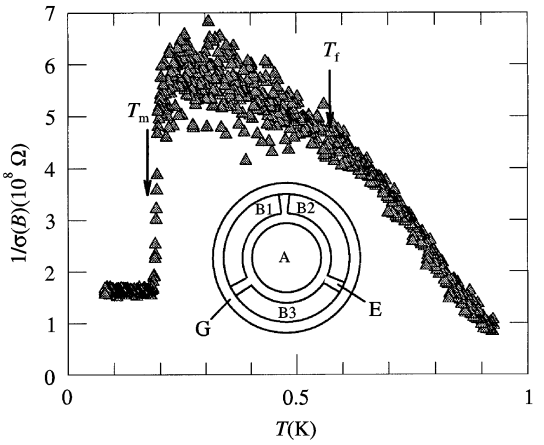

Fig. 6. The temperature dependence of $1/\sigma(B)$ for $n = 0.74 \times 10^{12}\ \mathrm{m}^{-2}$, $B = 0.2$ T, $f = 4$ kHz and $V_0 = 10$ mV. Fluctuations occur between T_m and T_f.

model, $\sigma(B) \approx ne/\mu B^2$, in agreement with the theory. Below 0.7 K, the conductivity deviates from the theory and fluctuates until the sharp transition to the solid at T_m. These fluctuations are not noise but follow a straight-line locus on the Argand diagram consistent with fluctuating coupled and uncoupled domains, where the coupling is due to Bragg–Çerenkov scattering from the ripplons. The temperature dependence of the standard deviation of these fluctuations show that they start at a temperature $T_f = (2.8 \pm 0.3)\ T_m$ which scales as $n^{1/2}$ and T_m, corresponding to $\Gamma = 46 \pm 5$. Strong fluctuations are also observed in the solid at high drive amplitudes, above V_c, again suggesting coupled and uncoupled domains as the Hall velocity of some electrons exceeds the ripplon phase velocity v_1 [12]. Small fluctuations are found even at low drives in the solid, suggesting that a small fraction (2–5%), may be uncoupled in the crystal phase, possibly in supercooled grain boundaries, which could produce slip as discussed above.

5. Conclusions

Two-dimensional electrons above liquid helium form the simplest conductor but display a wealth of interesting physics. This is perhaps the first system where both Wigner crystallization, and also, as we show, the effects of strong electron correlations in the fluid phase have been observed. These effects give Drude behaviour of the electron conductivity in low B fields and the saturation and density dependence of $\sigma(B)$ at higher fields. Above 2 T, the magnetoconductivity does not change through melting. The many-electron theory of scattering via the fluctuational field is equivalent to the multi-phonon scattering in the solid. For electrons on helium, only in the high field limit are the collisions with short-range scatterers independent of the electron–electron interaction. Using the method of moments, we have quantified the accuracy of the self-consistent Born approximation (SCBA), which is excellent for gas–atom scattering but not so good for long-range ripplon scattering. Surprisingly, no effects are observed in the solid due to the coupling of the transmission line mode to the diffusive shear mode, which suggests that the rotation of the solid produces a polycrystalline microstructure which relieves the shear stress by slip. In low fields in the solid on ^{4}He, $\sigma(B)$ is non-linear due to the Bragg–Çerenkov radiation of coherent ripplons which limits the Hall velocity to the phase velocity of the ripplons at the first reciprocal lattice vector. Above a threshold drive voltage, the conductivity decreases sharply. Fluctuations in $\sigma(B)$ are observed above T_m, up to a temperature $T_f = (2.8 \pm 0.3)\ T_m$ and suggest Bragg–Çerenkov coupled domains in the 2D electron fluid. Similar fluctuations are also observed at high voltage drives in the 2D solid.

Acknowledgements

We thank K. Djerfi, P. Fozooni, J. Frost, A. Kristensen, P.J. Richardson, A. Santrich-Badal and A.O. Stone, with whom many experiments were performed; C. Fang-Yen, F. Kuehnel and Yu. G. Rubo with whom theoretical results were obtained; P.W. Adams, A.J. Dahm, K. Kono, Yu. Z. Kovdrya, P.J.M. Peters, P.M. Platzman, J. Saunders, P.K.H. Sommerfeld, O. Tress and R.W. van der Heijden for useful discussions; the EPSRC (UK) for Research Grants; the EU for support under contract number CHRXCT 930374; A.K. Betts, F. Greenough, J. Taylor and A. Wilkinson for technical assistance; A. Blackburn, D. Murphy, A. Jury and other staff of the Southampton University Microelectronics Centre and the lithography unit

of the Rutherford Appleton Laboratory, UK, for electrode fabrication.

References

[1] E. Andrei (Ed.), Two-dimensional Electron Systems, Kluwer, 1997.
[2] G. Deville, J. Low Temp. Phys. 72 (1988) 135.
[3] M.I. Dykman, L.S. Khazan, Sov. Phys. JETP 50 (1979) 747.
[4] M.I. Dykman, C. Fang-Yen, M.J. Lea, Phys. Rev. B 55 (1997) 16249.
[5] C. Fang-Yen, M.I. Dykman, M.J. Lea, Phys. Rev. B 55 (1997) 16272.
[6] M.J. Lea, P. Fozooni, A. Kristensen, P.J. Richardson, K. Djerfi, M.I. Dykman, C. Fang-Yen, A. Blackburn, Phys. Rev. B 55 (1997) 16280.
[7] Yu. P. Monarkha, S. Ito, K. Shirahama, K. Kono, Phys. Rev. Lett. 78 (1997) 2445. In the theoretical analysis the authors mistakenly set $\langle 1/\boldsymbol{E}_f \rangle = 1/\langle \boldsymbol{E}_f^2 \rangle^{1/2}$, and the related part of their conclusions are wrong.
[8] S. Ito, K. Shirahama, K. Kono, J. Phys. Soc. Japan 66 (1997) 533.
[9] M.I. Dykman, M.J. Lea, P. Fozooni, J. Frost, Phys. Rev. Lett. 70 (1993) 3975.
[10] M.J. Lea, P. Fozooni, P.J. Richardson, A. Blackburn, Phys. Rev. Lett. 73 (1994) 1142.
[11] A. Kristensen, K. Djerfi, P. Fozooni, M.J. Lea, P.J. Richardson, A. Santrich-Badal, A. Blackburn, R.W. van der Heijden, Phys. Rev. Lett. 77 (1996) 1350.
[12] M.I. Dykman, Yu. G. Rubo, Phys. Rev. Lett. 78 (1997) 4813.
[13] K. Djerfi, P. Fozooni, S. Harris, M.J. Lea, P.J. Richardson, A. Santrich-Badal, R. van Haren, A. Blackburn, Phys. Rev. Lett. 80 (1998) 806.
[14] K. Shirahama, S. Ito, H. Suto, K. Kono, J. Low Temp. Phys. 101 (1995) 439.
[15] K. Shirahama, O.I. Kirichek, K. Kono, Phys. Rev. Lett. 79 (1997) 4218.
[16] Y. Iye, J. Low Temp. Phys. 40 (1980) 441.
[17] O. Tress, Ph.D. thesis, University of Konstanz, Magnetopolarons and Magnetoconductivity of Two-Dimensional Surface Electrons on the Surface of Bulk Helium and Helium Films, Hartung - Gorre, Konstanz, 1997.
[18] P.J. Richardson, Ph.D. thesis, University of London, 1997.
[19] P. Fozooni, P.J. Richardson, M.J. Lea, M.I. Dykman, C. Fang-Yen, A. Blackburn, J. Phys.: Condens. Matter 8 (1996) L215.
[20] P.J.M. Peters, P. Scheuzger, M.J. Lea, Yu. P. Monarkha, P.K.H. Sommerfeld, R.W. van der Heijden, Phys. Rev. B 50 (1994) 11570.
[21] M. Saitoh, J. Phys. Soc. Japan 42 (1977) 201.
[22] F. Kuehnel, M.I. Dykman, in preparation.
[23] M.I. Dykman, J. Phys. C. 15 (1982) 7397.
[24] M. Saitoh, J. Phys. Soc. Japan 56 (1984) 706.
[25] K. Djerfi, P. Fozooni, M.J. Lea, A. Santrich-Badal, private communication.
[26] Yu. G. Rubo, M.J. Lea, Phys. Rev. B (1998).
[27] K. Shirahama, K. Kono, Phys. Rev. Lett. 74 (1995) 781.
[28] L. Wilen, R. Giannetta, Solid State Commun. 78 (1991) 199.
[29] K. Shirahama, S. Ito, H. Suto, K. Kono, J. Low Temp. Phys. 101 (1995) 433.
[30] K. Shirahama, K. Kono, J. Low Temp. Phys. 104 (1996) 237.